PERGAMON

International Journal of Solids and Structures 37 (2000) 3569–3589

INTERNATIONAL JOURNAL OF SOLIDS and STRUCTURES

www.elsevier.com/locate/ijsolstr

The toppling of hanging beams

T.J. Stratford, C.J. Burgoyne*

Department of Engineering, University of Cambridge, Trumpington Street, Cambridge CB2 1PZ, UK

Received 27 August 1998; in revised form 25 February 1999

Abstract

This paper considers the behaviour of beams hanging from cables. If heavy, these beams can topple sideways in a mode which can be idealised as a rigid body rotation, combined with a minor axis deflection. This simplification allows an analytical treatment of the toppling mode, which in turn allows a stability analysis of heavy beams, such as prestressed precast concrete bridge beams. A detailed analysis is presented for beams with inclined or vertical cables, with inclined or vertical lifting yokes, with lateral loads (as from wind or inertia effects), and with initial imperfections. Examples are given of the various effects that can be analysed in this way, and the validity of the initial assumption, about rotation without variation in twist, is checked. It is shown that this type of analysis is particularly suited to concrete beams.

1. Introduction

The lateral stability of precast concrete bridge beams is a potential problem if current production techniques are extended to longer spans. The need to keep weight down for transportation, while increasing spans to deal with wider roads, has meant that the beams tend to have only residual flanges. They thus become susceptible to lateral buckling. However, unlike steel beams, for which lateral–torsional buckling is a well-known problem, with modern concrete beams the torsional stiffness is of the same order of magnitude as the minor axis stiffness (rather than being an order of magnitude lower), and the primary loading case to be considered is the beam's own self-weight.

In a separate study, using finite element techniques (Stratford and Burgoyne, 1999), it was found that the case of the beam hanging from cables was the most critical condition, due to the absence of any rotational restraint, and also that the relatively high torsional stiffness means that the beam tends to rotate as a rigid body, with very little variation of twist along the length. Thus, the buckling mode of a

* Corresponding author. Fax: +44-1223-332662.
E-mail address: cjb@eng.cam.ac.uk (C.J. Burgoyne).

0020-7683/00/$ - see front matter
PII: S0020-7683(99)00059-1

Nomenclature

a	Distance of yoke attachment point from end of beam
b	Distance of yoke attachment point from centre of beam
C, D	Used in hanging beam analysis to simplify equations.
C_D	Drag Coefficient
d	Overall beam depth
e	Position of action of p on beam below the yoke to cable attachment points
E	Young's modulus of concrete
F	Tension in cables
G	Shear Modulus of concrete
H	Axial load in beam due to horizontal component of cable tension
h	Height of yoke to cable attachment points above the centroid of the beam
I_x	Second moment of area about the beam section's major-axis
I_y	Second moment of area about the beam section's minor-axis
J	St. Venant's torsion constant for beam section
L	Length of beam
M	Bending moment about minor-axis of beam
M_Z	Moment of cable forces about the minor-axis at the yoke attachment point
M_0	All minor-axis moments acting about the yoke attachment point
p	Lateral load on beam per unit length
P_{cr}	Euler buckling load of beam
T	Torque in beam
$v(x)$	Lateral deflection measured in the minor-axis direction (which rotates with θ)
v', v''	First and second differentials of $v(x)$ with respect to position (dv/dx, d^2v/dx^2)
V	Component of the cable tension acting parallel to the major-axis of the beam
$v_0(x)$	Shape of initial imperfection
V_S	Wind speed
V_0	Minor-axis shear force in beam just inside yoke attachment points
v_{ms}	Mid-span lateral deflection along minor axis of beam
w	Self weight of beam per unit length
w_{cr}	Critical self weight of beam to cause buckling per unit length
x	Distance along beam, measured from the yoke attachment point
y_b	Distance of bottom fibre of beam below centroid of beam
α	Cable inclination angle above the horizontal
β	Yoke inclination angle above the horizontal
χ	Used in hanging beam analysis to simplify equations.
δ_0	Magnitude of initial lateral imperfection
λ	Slope of beam at $x = 0$
κ_{ms}	Mid-span curvature about minor-axis
κ_0	Initial mid-span curvature
μ	Axial load parameter in hanging beam buckling analysis.
$\delta\theta$	Twist in beam about axis
θ	Roll angle: rigid body rotation about the beam's axis
ρ	Density of air
ψ	Lateral load parameter

hanging concrete beam can be regarded, to a large degree, as a lateral bending of the beam about its minor axis, combined with a rigid body rotation about the points of attachment to the supporting cables.

The phrase '*toppling*' will be used in this paper to refer to such a rigid body rotation, to distinguish it from '*twisting*', which is taken to imply a variation of rotation along the length of the beam.

The complete lateral–torsional buckling problem of a beam supported by cables is not amenable to analytical solution. The cables may be inclined to the vertical, thus inducing axial forces in the beam; they may not be attached at the ends of the beam, and they will certainly not be attached on the centroidal axis. However, by assuming that the beam does not twist (by effectively assuming infinite torsional rigidity), the problem is simplified, and an analytical solution becomes possible, albeit one which requires the numerical solution of a final set of equations. That analysis is the subject of this paper.

Swann and Godden (1966) investigated the lateral buckling of concrete beams lifted by cables and presented a numerical method for determining how they behave. Baker and Edwards (1985) gave a method for analysing the non-linear elastic behaviour of thin-walled reinforced and prestressed beams which might be used to analyse the stability of various support conditions. However in both cases the analysis is complicated and neither paper leads to a simple design formula. Mast (1989, 1993) (also reported by Anderson, 1971) gave a simple analysis, but this does not treat inclined cables or initial imperfection effects in detail.

2. Definition of problem

Fig. 1 shows the generic problem. A beam of length L is supported at a distance a from each end by two yokes ZY and Z′Y′, which are rigidly attached to the beam and are inclined at an angle β to the centroidal axis. The half-distance between the supports is b. The tops of the yokes are attached to cables which are inclined at an angle α and meet at X. In practice, β will either be 90° if the yokes are prevented from rotating about a horizontal axis, or be equal to α if the yokes can align with the cables. The derivation will be carried out for a general value of β, which can then simplified for the two special cases. The cables are attached to the yokes at a height of h above the centroidal axis.

The only loads acting on the beam are the self-weight w per unit length, which acts at the centroid, and a load p per unit length which acts normal to the beam. This force is assumed to be made up of

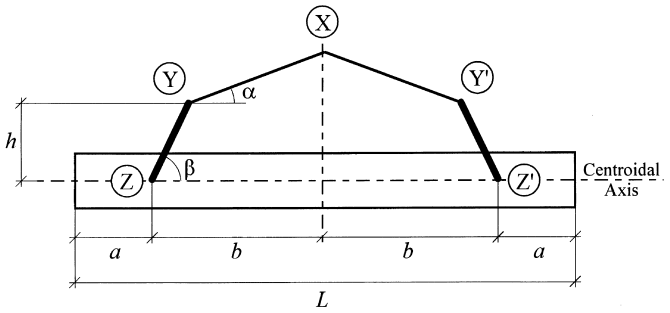

Fig. 1. The undeformed geometry of a beam hanging from inclined yokes and cables.

two components; wind loads which act at the mid-height of the beam and dynamic factors which act at the centroid. These are combined: the analysis assumes that both act through a single point at a distance e below the top of the yokes, Y and Y′.

3. Outline of theory

Fig. 2 shows the buckled shape of a hanging beam. The shape is defined by a rigid-body rotation through an angle θ, together with a deflection, $v(x)$ measured along the minor-axis direction (which itself rotates with θ) as shown in Fig. 3. $v(x)$ is measured relative to the centroid of the beam at the point where the cables are attached. The variable x is measured (without loss of generality) from the left-hand yoke attachment point.

4. Assumptions

The following assumptions are made:

1. The beam does not deflect by bending about its major-axis or by torsion. However, it is free to bend about its minor-axis and to topple as a rigid-body.
2. The yokes are assumed to be rigid and to be rigidly connected to the beam.
3. The tops of the yokes are attached (at Y and Y′) to cables which are inclined at an angle α to the horizontal and which meet at a point X. The cables can only carry axial tensile force.
4. The beam has a small initial imperfection $v_0(x)$ which varies as a single sinusoidal half wave along the beam's length, but offset so that $v_0 = 0$ at the yoke attachment points.
5. The beam is acted on by a lateral load p per unit length, which is applied at a distance e below the yoke-cable attachment points. p is assumed to act parallel to the direction of the beam's major principal axis as the beam rotates.
6. The beam's own self-weight acts through the centroid.
7. The minor-axis deflection v is assumed to be small by comparison with the length of the beam.
8. The beam remains linear elastic at all times with fixed section properties.

The assumption about fixed stiffnesses means that the analysis does not attempt to look at the behaviour of the beam after cracking takes place. Cracking would significantly reduce the stiffness of the

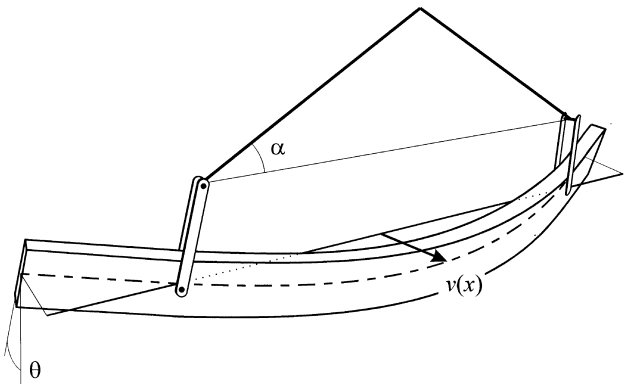

Fig. 2. The buckling mode of a typical beam hanging from inclined cables showing the parameters used to define its shape.

beam; if buckling was imminent before cracking it would certainly occur after cracking, which would thus be catastrophic. The results of this analysis are used elsewhere (Stratford and Burgoyne, 1999) to give design guidance, with particular attention paid to the stresses induced by the pre-buckling deformations. These can then be compared with the prestress to ensure that cracking does not occur. Thus, in the present analysis, not only must the critical load be determined, but also the response to initial imperfections. The maximum lateral displacement will be used in a Southwell plot analysis and the maximum minor-axis curvature will be used to impose limits on the minor axis bending stresses that are induced.

5. General analysis

Fig. 4 shows a vertical section through the beam at one of the yoke attachment points.

The cables are inclined at an angle to the vertical due to the action of the lateral load p. The cable tension F can be found by applying the cosine rule to the force polygon shown in the inset in Fig. 4:

$$F = \frac{L\sqrt{w^2 + p^2 + 2wp\sin\theta}}{2\sin\alpha}. \tag{1}$$

Consideration of moment equilibrium for the whole beam about an axis through YY′ leads to:

$$wh\sin\theta + pe + \frac{wh\lambda\cos\theta}{\tan\beta} = \frac{w\cos\theta}{L}\int_{\text{length}} v\,\mathrm{d}x, \tag{2}$$

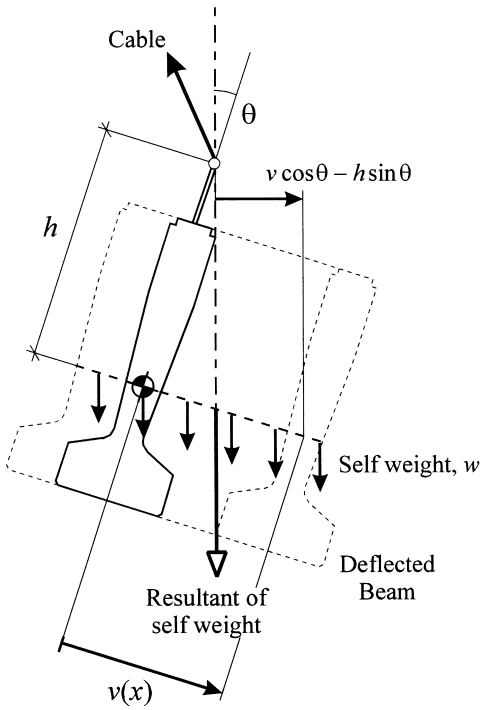

Fig. 3. A vertical section through the beam at a yoke attachment point, showing the displacements.

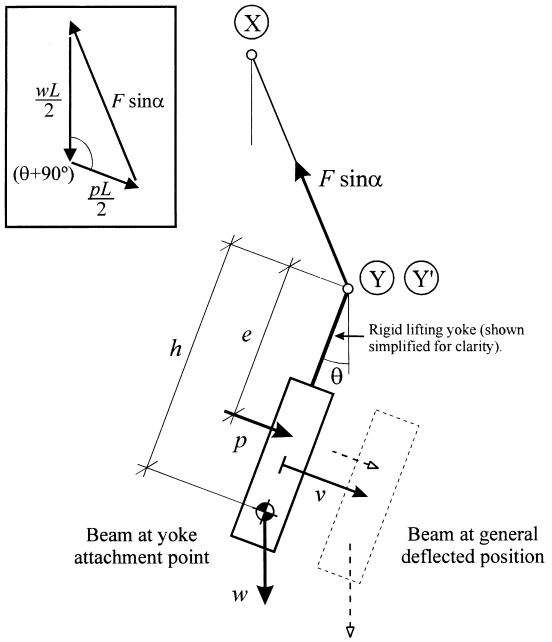

Fig. 4. The forces acting on a deflected hanging beam.

in which the third term represents a correction factor, which cannot easily be visualised in Fig. 4, that accounts for the lateral change in position of YY′ when the yokes are not vertical and when the beam is bending about the minor axis. λ is defined as the minor-axis slope of the beam at the yoke attachment point Z,

$$\lambda = (v')_{x=0} \tag{3}$$

(Primes denote differentiation with respect to x).

Eq. (2) will later be used to establish the roll angle θ as a function of the displaced shape v.

Fig. 5 shows the deflected shape of the beam in the minor-axis direction, including the initial sinusoidal imperfection v_0 of magnitude δ_0:

$$v_0 = \delta_0 \sin\frac{\pi(x+a)}{L} - \delta_0 \sin\frac{\pi a}{L}. \tag{4}$$

Note that for convenience, x is measured relative to the left hand yoke attachment point Z.

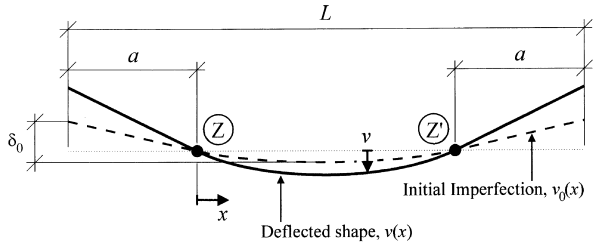

Fig. 5. The minor-axis deflected shape of the beam, and the initial imperfection.

Fig. 6 shows all the forces acting on the beam: the cable tension F, the beam's self-weight w, and the lateral loading p, while Fig. 7 shows the components of these forces which act in the axial and minor-axis directions, since the analysis is concerned only with the actions that cause bending about the beam's minor-axis, the section being deemed to be rigid for both major-axis bending and torsion. For clarity the beam has been shown with the minor axis horizontal, and with no curvature. The component of the self-weight which acts laterally is $w \sin\theta$. V and H are the components of the cable tension which act in the minor-axis and axial directions respectively. By resolving forces laterally:

$$V = \frac{(w \sin\theta + p)L}{2}. \tag{5}$$

The axial component of the cable tension is $H = F\cos\alpha$, where F is given in Eq. (1):

$$H = \frac{L\sqrt{w^2 + p^2 + 2wp\sin\theta}}{2\tan\alpha} \tag{6}$$

In Fig. 8, these forces are transferred to the beam's centroid. It is convenient to express the total lateral distributed load as ψ:

$$\psi = w\sin\theta + p. \tag{7}$$

The moment of the cable forces (V and H) about the yoke attachment points (Z and Z′) is M_Z. This is obtained by considering Fig. 9, which shows the deflected shape of the beam and the cable forces acting at the top of the yokes (Y and Y′). Taking moments about Z gives:

$$M_Z = \frac{h}{\tan\beta}(V + \lambda H). \tag{8}$$

It is convenient to derive the governing differential equation by considering the beam between the two yoke attachment points (Z and Z′) by itself, as shown in Fig. 10. The effect of the lateral loading on the overhangs (outside the section Z to Z′) must be included in the moment at the end of this section M_0. Using Eq. (8):

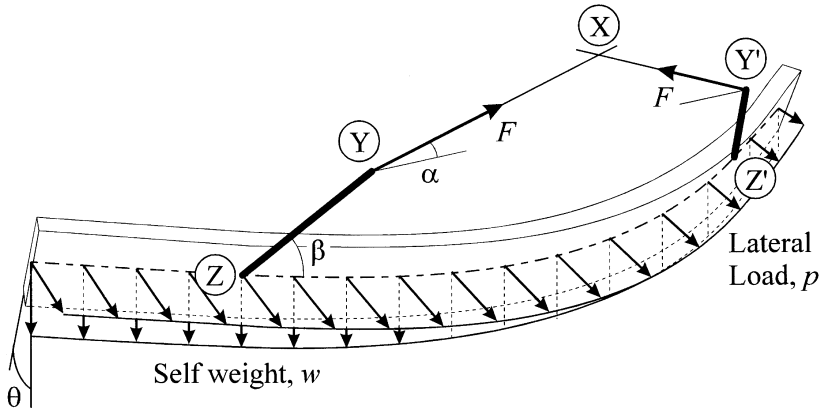

Fig. 6. The forces acting on a hanging beam, in three dimensions.

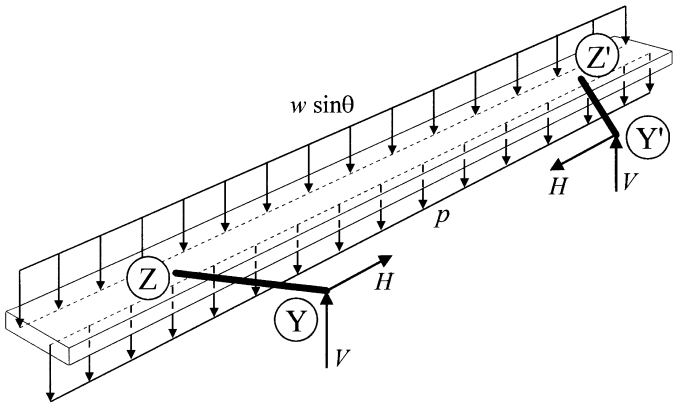

Fig. 7. Simplified view showing only those loads which cause minor-axis bending of a hanging beam. The beam is shown with its major axis horizontal and undeformed for clarity.

$$M_0 = \left(M_Z + \frac{\psi a^2}{2}\right) = \frac{h}{\tan\beta}(V + \lambda H) + \frac{\psi a^2}{2}. \tag{9}$$

The shear force at the end of the section Z–Z', V_0 is simply:

$$V_0 = \psi b. \tag{10}$$

The remainder of the solution depends on whether the cables are inclined or vertical, since this affects the form of the governing differential equation.

6. Beams with inclined cables

The governing equation for buckling in the central section of beam with inclined cables, as shown in Fig. 10, is:

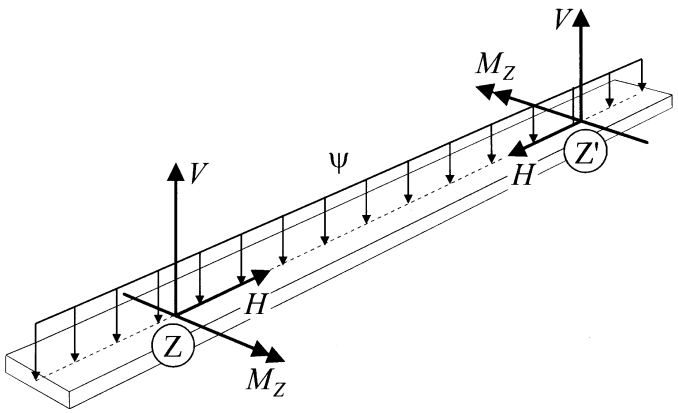

Fig. 8. The forces which give minor-axis bending transferred to the beam's centroid.

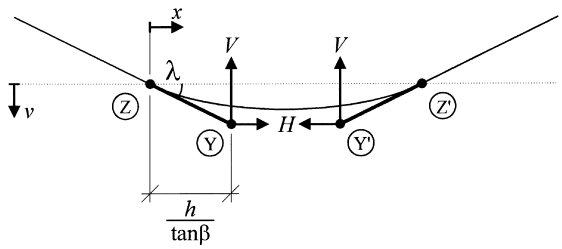

Fig. 9. Determination of the moment about the yoke attachment points due to the cable forces acting at the ends of the yokes.

$$M = -EI_y\left(v'' - v_0''\right) = V_0 x - \frac{\psi x^2}{2} + Hv - M_0. \tag{11}$$

This can be solved to give:

$$v = A\cos\mu x + B\sin\mu x + \frac{1}{\mu^2 EI_y}\left[\psi\left(\frac{x^2}{2} - \frac{1}{\mu^2}\right) - V_0 x + M_0\right] + \frac{\pi^2\delta_0}{\pi^2 - \mu^2 L^2}\sin\frac{\pi(x+a)}{L}, \tag{12}$$

where

$$\mu = \sqrt{\frac{H}{EI_y}} \tag{13}$$

and A and B are constants.

The boundary conditions $v = 0$ at $x = 0$ and $v' = 0$ at $x = b$ (mid-span) allow A and B to be calculated, whence:

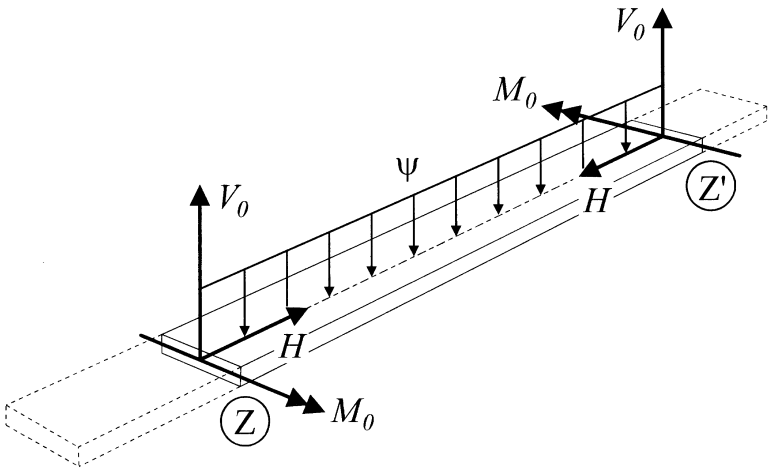

Fig. 10. The forces acting on the central section of the beam, used to derive the governing equation for buckling.

$$v =$$

$$\frac{\psi}{\mu^4 EI_y}\left[\left(1-\frac{M_0\mu^2}{\psi}\right)(\cos\mu x+\tan\mu b\sin\mu x-1)+\mu^2\left(\frac{x^2}{2}-bx\right)\right]$$

$$+\frac{\pi^2\delta_0}{\pi^2-\mu^2L^2}\left[\sin\frac{\pi(x+a)}{L}-\sin\frac{\pi a}{L}(\cos\mu x+\tan\mu b\sin\mu x)\right] \tag{14}$$

(for $0 \le x \le 2b$).

Note that this is not a complete solution in its own right since it implicitly still involves the roll angle θ through the lateral load variable ψ (via Eq. (7)).

Eq. (14) describes the deflected shape of the beam between the yokes. It is also necessary to establish the deflected shape in the overhangs; this is a simple bending problem (since no axial force is present) with the governing equation:

$$M = -EI_y\left(v''-v_0''\right) = -\frac{\psi(a+x)^2}{2}. \tag{15}$$

This is solved subject to the boundary conditions $v = 0$ at $x = 0$ and $v' = \lambda$ at $x = 0$. This second condition ensures continuity of slope between the overhangs and the central section. The shape of the deflected overhangs is:

$$v = \frac{\psi}{EI_y}\left[\frac{(a+x)^4}{24}-\frac{a^3x}{6}-\frac{a^4}{24}\right]+\delta_0\left[\sin\frac{\pi(x+a)}{L}-\frac{\pi x}{L}\cos\frac{\pi a}{L}-\sin\frac{\pi a}{L}\right]+\lambda x \tag{16}$$

(for $-a \le x \le 0$).

λ is obtained by differentiating the equation for the shape of the central section Eq. (14) and setting $x = 0$:

$$\lambda = \frac{\psi}{\mu^4 EI_y}\left[\left(1-\frac{M_0\mu^2}{\psi}\right)\mu\tan\mu b-\mu^2 b\right]+\frac{\pi^2\delta_0}{\pi^2-\mu^2L^2}\left[\frac{\pi}{L}\cos\frac{\pi a}{L}-\mu\sin\frac{\pi a}{L}\tan\mu b\right]. \tag{17}$$

Eqs. (14) and (16) between them give the deflected shape of the beam throughout its length in terms of the roll angle θ. Eq. (2) describes the overall equilibrium of the beam and can be used to obtain a solution in terms of the roll angle θ only. To apply Eq. (2), it is necessary to integrate the deflected shape along the length of the beam. Since the mode shape is symmetrical, it is convenient to express this integral as:

$$\underset{\text{length}}{\int v\,\mathrm{d}x} = \underset{\text{overhangs}}{2\int_{-a}^{0} v\,\mathrm{d}x} + \underset{\text{central section}}{\int_0^{2b} v\,\mathrm{d}x}. \tag{18}$$

Eq. (18) can be evaluated by integrating Eqs. (14) and (16), and substituting for λ from Eq. (17). The resulting expression for $\int_{\text{length}} v\,\mathrm{d}x$ is then used in Eq. (2) to give:

$$\left(h\sin\theta+\frac{p}{w}e\right) = C\cos\theta(w\sin\theta+p)+D\cos\theta, \tag{19}$$

where:

$$C = \frac{1}{\mu^4 EI_y L}\left[\left(\frac{1}{\mu} - \frac{\mu M_0}{\psi}\right)(\chi - 2\mu b) + \mu^2 a^2 b - \frac{2}{3}\mu^2 b^3 + \frac{a^5\mu^4}{10} - \frac{\mu^2 hL}{\tan\beta}\left(\left(\frac{1}{\mu} - \frac{\mu M_0}{\psi}\right)\tan\mu b - b\right)\right],$$

$$D = \frac{\pi^2\delta_0}{(\nu^2 - \mu^2 L^2)L}\left[\frac{L}{\pi}\left(2 - \frac{a^2\pi^2}{L^2}\right)\cos\frac{\pi a}{L} - \frac{\chi}{\mu}\sin\frac{\pi a}{L} - \frac{hL}{\tan\beta}\left(\frac{\pi}{L}\cos\frac{\pi a}{L} - \mu\sin\frac{\pi a}{L}\tan\mu b\right)\right]$$

$$+2\frac{\delta_0}{L}\left[\left(\frac{\pi a^2}{2L} - \frac{L}{\pi}\right)\cos\frac{\pi a}{L} - a\sin\frac{\pi a}{L} + \frac{L}{\pi}\right] \tag{20}$$

and

$$\chi = \sin 2\mu b + \tan\mu b(1 - \cos 2\mu b - a^2\mu^2). \tag{21}$$

Note that the above equations are dependent upon the end moment M_0. Eq. (9) gives a relationship for M_0 in terms of λ (itself a function of M_0). By substituting for λ from Eq. (17), in Eq. (9) and rearranging:

$$M_0 = \frac{1}{\tan\beta + h\mu\tan\mu b}\left[\psi\left(h\left(\frac{L}{2} + \frac{\tan\mu b}{\mu} - b\right) + \frac{a^2\tan\beta}{2}\right)\right.$$
$$\left. + \frac{\delta_0\pi^2\mu^2 hEI_y}{(\pi^2 - \mu^2 L^2)}\left(\frac{\pi}{L}\cos\frac{\pi a}{L} - \mu\sin\frac{\pi a}{L}\tan\mu b\right)\right]. \tag{22}$$

Substitution of Eqs. (20)–(22) into Eq. (19) gives an equation in which the only unknown is the roll angle θ. In general, no analytical solution exists, but it can be solved by a suitable numerical technique, such as Newton–Raphson. The aim is to find the value of θ which, when substituted into Eqs. (6), (13) and (20)–(22) leads to Eq. (19) being satisfied. The process is tedious, but essentially straightforward. The deflected shape can then be found using Eqs. (14) and (16). Alternatively, θ can be fixed and w varied until Eq. (19) is satisfied. All of the results in this paper were produced in one or other of these ways using the solver routine on a spreadsheet.

Of particular interest is the mid-span deflection, v_{ms}. From Eq. (14) with $x = b$:

$$v_{ms} = \frac{\psi}{\mu^4 EI_y}\left[\left(1 - \frac{M_0\mu^2}{\psi}\right)(\cos\mu b + \tan\mu b\sin\mu b - 1) - \frac{\mu^2 b^2}{2}\right]$$
$$+ \frac{\pi^2\delta_0}{\mu^2 - \mu^2 L^2}\left[1 - \sin\frac{\pi a}{L}(\cos\mu b + \tan\mu b\sin\mu b)\right]. \tag{23}$$

It is also useful to calculate the mid-span curvature. By differentiation of Eq. (14), this can be conveniently expressed in terms of v_{ms}:

$$\kappa_0 + \kappa_{ms} = \mu^2 v_{ms} + \frac{1}{EI_y}\left(\frac{b^2\psi}{2} - M_0\right) + \frac{\delta_0\pi^2}{L^2}. \tag{24}$$

Note that Eq. (24) includes the initial curvature, $\kappa_0 = \delta_0\pi^2/L^2$. To calculate the additional stresses caused by lifting (over and above those due to the imperfection), the additional curvature is given by:

$$\kappa_{ms} = \mu^2 v_{ms} + \frac{1}{EI_y}\left(\frac{b^2\psi}{2} - M_0\right). \tag{25}$$

Eqs. (6) and (13) and Eqs. (19)–(25) are the complete general solution to the hanging beam problem. For a given beam, the roll angle θ is found from Eq. (19) and then the mid-span deflection and mid-span curvature are found from Eqs. (23) and (25).

7. Simplifications

The general solution includes the effects of an initial imperfection, inclined yokes and lateral loading. In practice, it is unlikely that all these effects will require consideration at once. Useful special cases which yield considerably simplified solutions are given below. The numerical examples relate to the largest precast bridge beam available in the UK at present. This is from the Super-Y beam series (Precast Concrete Association), and is designated SY-6. It is designed for spans up to 40 m and has the section properties given in Table 1. All solutions have been obtained by assuming that the short-term modulus of elasticity of concrete is 34 kN/mm^2.

7.1. Perfect beam with vertical yokes and no lateral load

This is the simplest case with no initial imperfection ($\delta_0 = 0$), vertical yokes ($\beta = 90^\circ$) and no lateral load ($p = 0$). It thus gives the buckling load and post-buckling response of a beam with inclined cables. Fig. 11 compares the results of this analysis with the finite element eigenvalue solution described elsewhere (Stratford and Burgoyne, 1999). For larger values of h and for $0.1 < a/L < 0.25$, the present analysis slightly over-estimates the buckling load. This is to be expected, since this analysis has assumed the beam to be torsionally rigid; the actual torsional flexibility will allow buckling to occur at a slightly lower load than that produced by this simplification. However, since most beams are supported near their ends, this discrepancy will not usually be significant.

Above the critical load, the mid-span deflection can be found from Eq. (23). The short-dashed line on Fig. 12 shows the variation in post-buckling mid-span deflection with beam self-weight for a typical beam.

Table 1
Section properties of SY-6 beam

		SY-6 beam
Overall beam depth	d (m)	2[a]
Height of centroid above soffit	y_b (m)	0.855[a]
Cross sectional area	A (m^2)	0.709[a]
2nd moment of area about major-axis	I_x (m^4)	0.2837[a]
2nd moment of area about minor-axis	I_y (m^4)	0.0140[b]
St. Venant's torsion constant	J (m^4)	0.0221[c]
Self weight	w (kN/m)	16.74[a]

[a] From Precast Concrete Association Data Sheets.
[b] From simple hand analysis.
[c] From computer analysis.

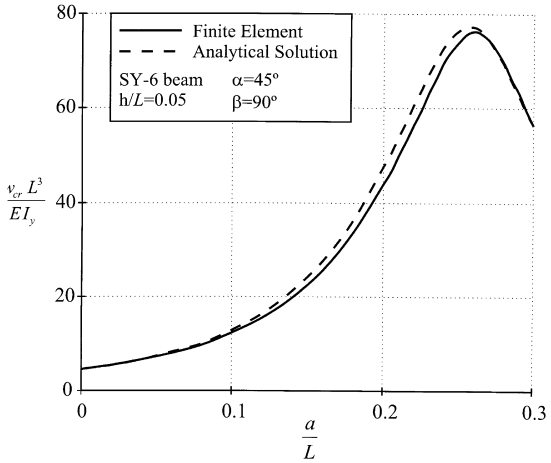

Fig. 11. Comparison of buckling load predictions obtained using the analytical solution with those of the eigenvalue finite element analysis.

7.2. Initially imperfect beam with vertical yokes and no lateral load

In this case, an initial imperfection of magnitude δ_0 is introduced. The yokes remain vertical ($\beta = 90°$) and there is no lateral load ($p = 0$). This analysis allows the imperfection sensitivity of the previous problem to be studied.

Results for a 40 m long SY-6 beam with a 30 mm initial imperfection are shown on Fig. 12. The imperfect results are asymptotic to the post-buckling perfect behaviour, as would be expected. The results are compared with a finite element initial imperfection analysis (Stratford and Burgoyne, 1999), and show close agreement.

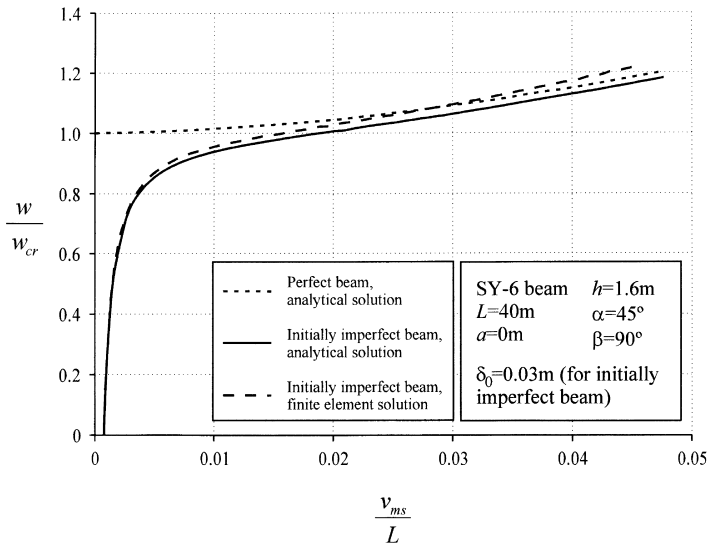

Fig. 12. Comparison of the load–deflection behaviour predicted using the analytical solution for a perfect beam with the results of the finite element analysis, for an initially imperfect beam.

7.3. Perfect beam with inclined yokes and no lateral load

In this case, the yokes are allowed to line up with the lifting cables ($\beta = \alpha$). The beam is perfect ($\delta_0 = 0$) and there is no lateral load ($p = 0$). The problem thus represents the critical loading case for beams where the yokes are free to rotate to match the inclination of the cables.

Fig. 13 shows the effect of allowing the yokes to rotate and of varying α, for a beam supported at its ends. When $\beta = \alpha$, so that the yokes align with the cables, the effect of increasing α is to slightly increase the critical load, whereas when β is fixed at 90°, so that the yokes are vertical, the critical load decreases. This result is slightly counter-intuitive, since at first sight inclining the cables induces an axial force, which can be expected to decrease the critical load, but there is a second factor, in that the effective points of support (the positions of Y and Y′) move in from the ends and are displaced laterally. This is a result which should be checked by model testing. It is important to note that this result relies on the rigidity of the yoke connections, since a small amount of flexibility in the yoke causes a significant movement in the position of the cable connection, and hence of the axis of rotation.

The general equations can be used to investigate the behaviour of an imperfect beam with inclined yokes.

7.4. Laterally loaded, end supported, initially imperfect beam with vertical yokes

This problem corresponds to the case of a hanging beam with a lateral wind load applied. The effect will be to cause minor-axis deformation, so the beam will deform non-linearly as soon as it is loaded. It is assumed that a lateral load p is applied to a beam with initial imperfection δ_0. To simplify the result, an end supported beam ($a = 0$) with vertical yokes ($\beta = 90°$) is considered.

Fig. 14 shows the results of such an analysis for a 40 m long beam supported at its ends, with a lateral pressure induced by wind. The pressure p induced by a wind speed of V_S is

$$p = \frac{1}{2} C_D \rho d V_S^2, \tag{26}$$

where ρ is the density of air (1.225 kg/m^3), C_D is the drag coefficient (=2.0 for a section like an I-beam

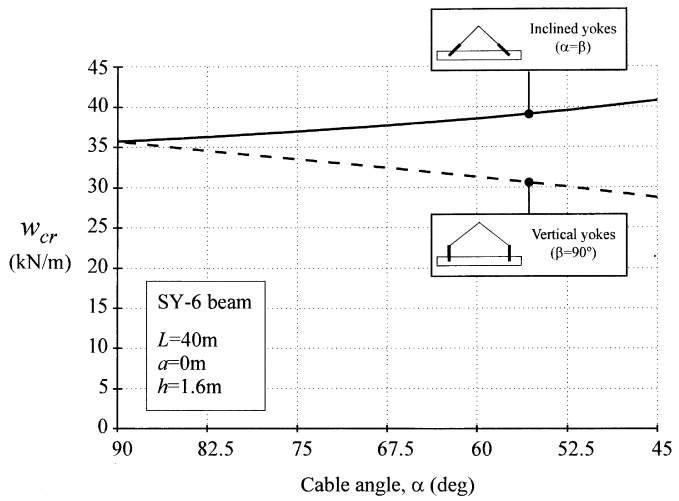

Fig. 13. Effect of allowing the yokes to rotate in line with inclined cables.

[Hoerner, 1965]) and d is the overall depth of the beam. Thus, for a 2 m deep beam in a wind speed of 20 m/s, $p = 0.98$ kN/m, while a 40 m/s wind induces a load of 3.92 kN/m. In the example, this is taken to act at the mid-depth of the beam, so that $e = 1.455$ m. The effect of the lateral load is to induce additional lateral deflection, which would cause additional minor axis bending stresses in the beam. There may, of course, be handling problems with hanging beams which would prevent operations with a crane at much lower wind speeds than these. Lateral forces can also be generated by inertial effects, for example when slewing the crane.

8. Beam hanging from vertical cables

When the beam is supported from vertical cables ($\alpha = 90^\circ$) there is no axial force, H, in the beam. This changes the form of the governing flexural differential equation Eq. (11) and the solution Eq. (12) is no longer valid. A separate simple bending analysis must be carried out. Note that only vertical yokes ($\beta = 90^\circ$) will be considered here since inclined yokes would have no function with vertical cables.

By considering Fig. 8 (and remembering that $H = 0$ and $V = \psi L/2$ from Eqs. (5) and (6)), the governing equation is:

$$M = -EI_y\left(v'' - v_0''\right) = \frac{\psi L}{2}\{x\} - \frac{\psi(x+a)^2}{2}. \tag{27}$$

This equation is valid both for the central section between the yoke attachment points and in the left overhang. The right overhang can be found by symmetry. The term $\psi L/2\{x\}$ includes a Macaulay bracket $\{\ldots\}$, since it describes the effect of the support reaction which only affects the bending moment when $x > 0$.

The governing equation is solved subject to $v = 0$ at $x = 0$ and $v' = 0$ at $x = b$ to give:

$$v = \frac{\psi}{48EI_y}\left[2(x+a)^4 - L^3x + 12b^2Lx - 2a^4 - 4L\{x\}^3\right] + \delta_0\left[\sin\frac{\pi(x+a)}{L} - \sin\frac{\pi a}{L}\right]. \tag{28}$$

The overall equilibrium equation Eq. (2) can be applied. The beam's deflected shape must be integrated over its length. Since the beam is symmetric, it is convenient to integrate over the left half of the beam only:

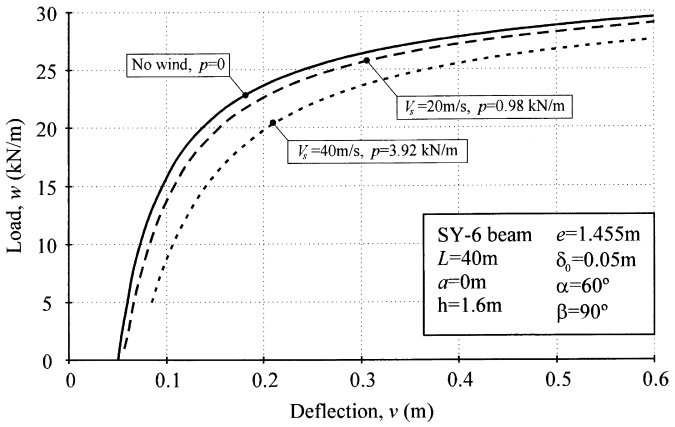

Fig. 14. Effect of lateral load (due to wind pressure) on the load deflection response.

$$\int_{\text{length}} v\,\mathrm{d}x = 2\int_{-a}^{b} v\,\mathrm{d}x. \tag{29}$$

Eq. (28) then gives an equation of the same form as a beam hanging from inclined cables:

$$\left(h\sin\theta + \frac{p}{w}e\right) = C\cos\theta(w\sin\theta + p) + D\cos\theta \tag{19 bis}$$

but with different constants, so that:

$$C = \frac{1}{12EI_y}\left[\frac{L^4}{10} - aL^3 + 3a^2L^2 - 2a^3L - a^4\right]$$

and

$$D = 2\delta_0\left[\frac{1}{\pi} - \frac{1}{2}\sin\frac{\pi a}{L}\right]. \tag{30}$$

Of particular interest is the mid-span deflection v_{ms}. From Eq. (28):

$$v_{\text{ms}} = \frac{\psi}{384EI_y}(5L^2 - 20aL - 4a^2)(2a - L)^2 + \delta_0\left(1 - \sin\frac{\pi a}{L}\right). \tag{31}$$

The mid-span curvature κ_{ms} is obtained by differentiation of Eq. (28):

$$\kappa_0 + \kappa_{\text{ms}} = \frac{\psi}{8EI_y}(L^2 - 4aL) + \frac{\delta_0\pi^2}{L^2}. \tag{32}$$

As for the case with inclined yokes, it is the additional curvature that is of interest, so:

$$\kappa_{\text{ms}} = \frac{\psi}{8EI_y}(L^2 - 4aL). \tag{33}$$

9. Simplifications

As with the solution for the inclined cables, it is possible to simplify the general solution for specific cases.

9.1. Perfect beam with no lateral load

This is the simplest case — the buckling load of a beam hanging from vertical cables — there is no initial imperfection ($\delta_0 = 0$), and no lateral load ($p = 0$).

As for a beam hanging from inclined cables, there is a critical load w_{cr} above which the beam will roll about its axis and buckle. By making suitable substitutions into Eqs. (19) and (30),

$$\frac{w_{\text{cr}}}{EI_y} = \frac{120h}{L^4\left(1 - 10\frac{a}{L} + 30\frac{a^2}{L^2} - 20\frac{a^3}{L^3} - 10\frac{a^4}{L^4}\right)}. \tag{34}$$

Mast (1989, 1993) derived a similar equation (if his factor of safety is set to unity), by checking for overturning of the beam. To include the effects of angled cables Mast modified this equation by the factor $(1-H/P_{cr})$ (where H is the axial compression in the beam due to inclined cables and P_{cr} is the Euler buckling load of the beam), and noted that this should be used with an appropriate safety factor. This modification and the present analysis agree well, but do not give identical results.

Fig. 15 shows the effect of varying the yoke position (as measured by a/L) for vertical cables ($\alpha=90^\circ$), and also for a variety of other values of α obtained from the inclined cable analysis given above. In all cases, the yokes are assumed to be vertical, so $\beta=90^\circ$. The significant increase in the buckling load that could be achieved by supporting the beam away from its ends is clearly visible, although for a prestressed beam, it is probably very unlikely that such a support condition would be allowable by virtue of the hogging bending that would be induced at the yoke attachment points.

Fig. 15 also shows, for the case of $\alpha=82.5^\circ$, the mode shapes that result for different support positions. The dramatic difference that occurs on either side of the peak is marked. When supported near the ends of the beam, the behaviour is for the centre of the beam to buckle sideways. When supported closer to the centre, the effect is for the ends of the beam to buckle, while the middle remains virtually straight.

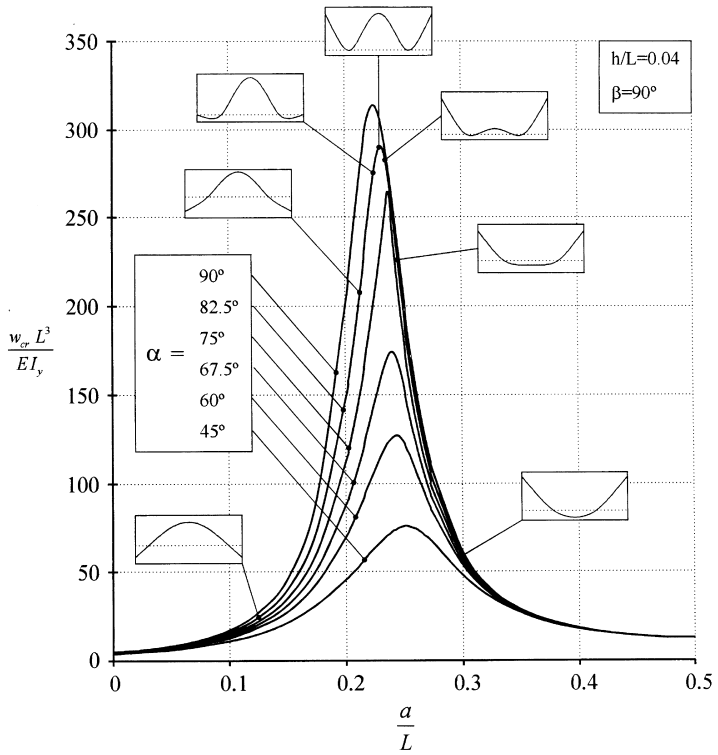

Fig. 15. Critical load of beams when supported at different positions and with cables of different inclinations. Inset figures show typical buckling modes.

9.2. Initially imperfect beam with no lateral load — interaction of buckling modes

The analysis is also capable of dealing with the complex behaviour that results when buckling modes interact. Fig. 16 shows the particular case of a beam with $a/L = 0.2375$, $\alpha = 75°$, $\beta = 90°$ and $h/L = 0.04$. This is close to the peak on Fig. 15. There are two, nearly adjacent, critical loads, as shown by the two solid lines, which represent the post-buckling paths for perfect beams. Also shown are paths followed by an imperfect beam, with $\delta_0/L = 0.00125$, and as insets some of the corresponding mode shapes. Not all of the imperfect paths would be stable. The way the mode shape changes at different portions of this complex curve can clearly be seen.

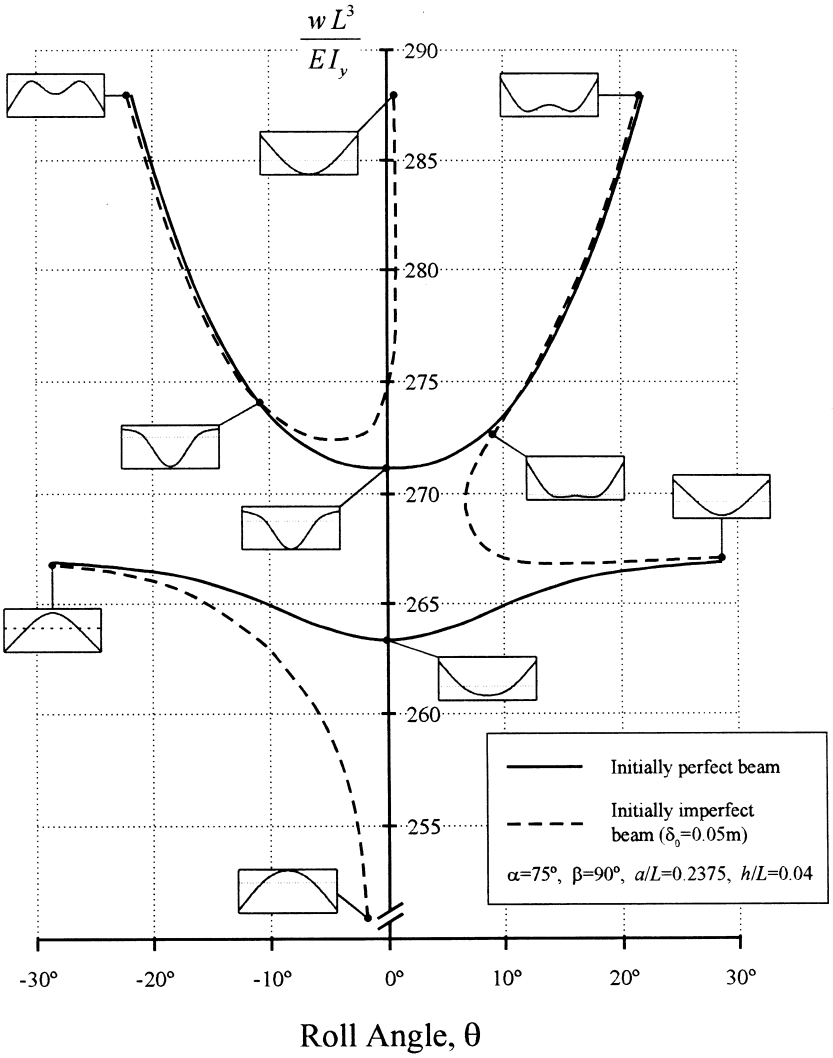

Fig. 16. Load deflection paths for a beam with two, closely adjacent, buckling loads. Inset figures show typical buckling modes.

10. Analysis of the twist

At the beginning of this analysis, the assumption was made that the beam rotated as a rigid body. It is possible to determine the reasonableness of that assumption (although not to correct it if it is false), by calculating the torque T along the length of the beam, and then integrating this to give the relative twist between the end of the beam and the centre. If this variation in twist is small by comparison with the toppling angle θ, then the assumption is valid.

Consideration of the forces acting on the beam, and its minor-axis displaced shape, allows the torque to be determined. This has to be done separately for the overhangs and the central portion.

In the left overhang ($x < 0$),

$$T = -p(x+a)(h-e) - \left[\frac{\psi}{EI_y}\left(\frac{x^5}{20} + \frac{ax^4}{4} + \frac{a^2x^3}{2} + \frac{a^3x^2}{2} + \frac{a^4x}{4} - \frac{a^5}{20}\right)\right] w\cos\theta \tag{35}$$

while, between the supports,

$$\begin{aligned} T = {} & -p(x+a)(h-e) + w\cos\theta\frac{\psi}{\mu^4 EI_y}\left\{\left[\left(1-\frac{M_0\mu^2}{\psi}\right)(\cos\mu x + \tan\mu b\sin\mu x - 1)\right.\right. \\ & \left.+\mu^2\left(\frac{x^2}{2} - bx\right)\right]\left(x + a - \frac{L}{2}\right) + \left[\left(1-\frac{M_0\mu^2}{\psi}\right)(-\mu\sin\mu x + \mu\tan\mu b\cos\mu x) + \mu^2(x-b)\right] \\ & \times\left(\frac{Hh}{w} + \frac{L}{2}\left(x - \frac{h}{\tan\beta}\right) - ax - \frac{x^2+a^2}{2}\right) - \left[\left(1-\frac{M_0\mu^2}{\psi}\right)\frac{1}{\mu}(\sin\mu x - \tan\mu b\cos\mu x - \mu x\right. \\ & \left.\left. + \tan\mu b) + \frac{\mu^2x^2}{2}\left(\frac{x}{3} - b\right)\right]\right\} + w\cos\theta\left[\frac{a^2\lambda}{2} - \frac{a^5\psi}{20EI_y} + \frac{Lh\lambda}{2\tan\beta}\right] + \frac{\psi Lh}{2}. \end{aligned} \tag{36}$$

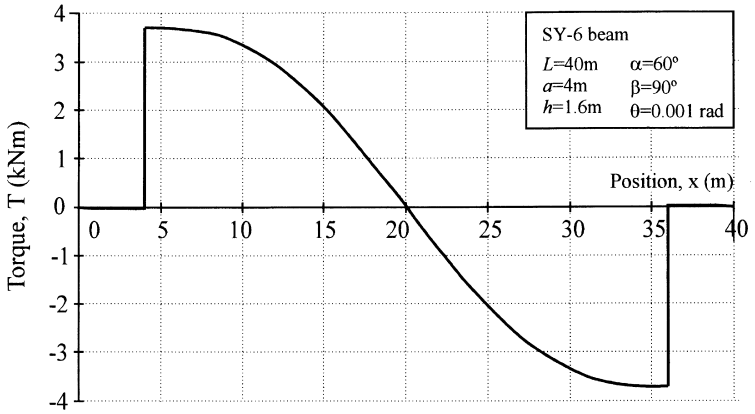

Fig. 17. Variation of torque along the length of a hanging beam.

The variation in torque that results from these equations can be seen in Fig. 17, which shows the case of a 40 m long SY-6 beam with $a = 4$ m. The torque must be zero at the ends of the beam, and also at the centre-line (by symmetry). If it is supported away from the ends, as in the figure, there will be a significant torque applied by the yokes. Note that the torque is a non-linear function of the roll angle θ (due to the $\cos\theta$ and $\sin\theta$ terms in Eqs. (35) and (36)), so this must be specified when determining the torque, but if there are no lateral loads, and θ is small, then it can be shown that $T \propto \theta$.

The rate of twist along the beam can then be determined from the torque, taking account of the torsional stiffness of the beam, and this can then be integrated to get the variation in twist ($\delta\theta$) between the ends of the beam and the centreline. It is possible to integrate Eqs. (35) and (36) analytically, but the resulting equations are very complex, and great accuracy is not required as this is simply a check on the validity of the original assumptions, so it is simpler to integrate numerically. When this is done for the case in Fig. 17, the variation in twist along the beam is 13% of the roll angle. This value increases when the beam is supported near the peaks shown on Fig. 15, but these peaks correspond to the beam buckling with very little rotation (so θ itself is small, as is $\delta\theta$). When the beam is supported at its ends, $\delta\theta/\theta$ is of the order of a few percent, so the assumption about a uniform toppling rotation was reasonable.

It is possible to obtain some comparative results for different sections which show why this analysis applies particularly to concrete beams, and not to steel beams. The torque shown in Fig. 17 has both positive and negative regions, which will tend to reduce the variation in twist along the beam. It will clearly be largest if all the torque is in the same sense, as would happen if the beam were supported at its ends. A beam with the dimensions shown in the inset of Fig. 18 was analysed. The beam has dimensions comparable with those of an SY-6 beam, but with the addition of flanges. By varying the width of these flanges, different ratios of torsional stiffness to minor axis stiffness can be obtained. Beams of this type were analysed, and for roll angles of 0.001 rad or 0.5 rad (0.06° or 28.6°), the twist variation was obtained and plotted against the ratio GJ/EI_y, as shown in the main part of Fig. 18.

For an SY-6 beam, for which $GJ/EI_y = 0.66$, the error in the roll angle is negligible, as it would be for

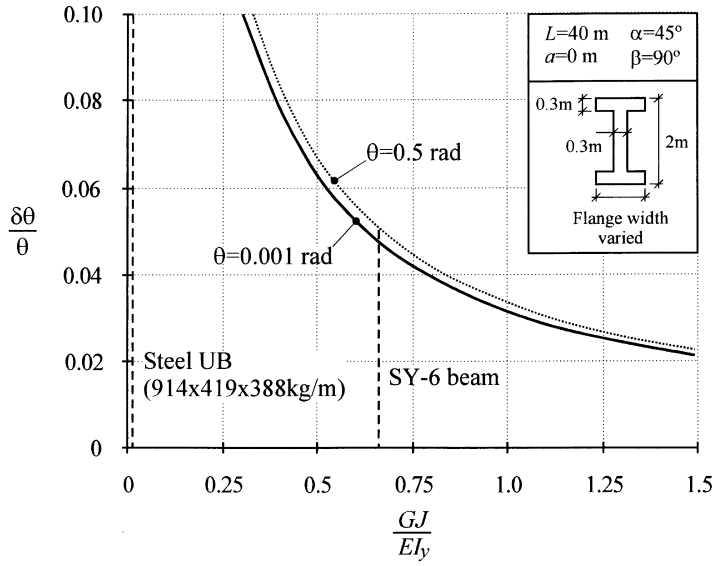

Fig. 18. Variation in twist between the ends and the centreline of a hanging beam.

most large, narrow concrete beams. Concrete beams with larger flanges would be unlikely to buckle under self-weight anyway, so the error in the analysis for those beams would not be important.

Open steel beams, on the other hand, for which GJ/EI_y will be an order of magnitude smaller, will have much larger errors, as illustrated by a 914 × 419 × 388 kg/m Universal Beam, for which $GJ/EI_y = 0.014$. These beams must be analysed using a more complex lateral–torsional buckling analysis, which is not needed for concrete beams. The present results may, however, be applicable to steel box sections, which are torsionally much stiffer.

11. Conclusions

The analysis presented here has shown that concrete beams can buckle laterally when hanging from a crane. This buckling mode can be imagined as a rigid-body rotation about the point of attachment of the cables, together with a minor-axis bending of the beam. Methods have been presented which show how the buckling load, the buckling mode, and the load–deflection path of imperfect beams can all be determined. Equations have been derived for both vertical cables and inclined cables. These can easily be solved using the solver routine in a spreadsheet, or by a similar numerical process. Various special cases have been examined to illustrate the capabilities of the method, and different ways in which it can be employed.

Simplified versions of these results, and recommendations for the stability design of long precast concrete beams, are presented elsewhere (Stratford et al., 1999).

Acknowledgements

The authors would like to thank Dr H.P.J. Taylor of Tarmac Precast Concrete Limited, and the Prestressed Concrete Association for their help with this project.

References

Anderson, A.R., 1971. Lateral stability of long prestressed concrete beams. PCI Journal 16, 7–9.

Baker, G., Edwards, A.D., 1985. A limit analysis of non-linear elastic displacements of thin-walled reinforced and prestressed beams. Engineering Structures 7, 198–203.

Hoerner, S.F., 1965. Fluid-Dynamic Drag: Practical Information on Aerodynamic Drag and Hydrodynamic Resistance. Published by the author, New Jersey.

Mast, R.F., 1989. Lateral stability of long prestressed concrete beams, Part 1. PCI Journal 34, 34–53.

Mast, R.F., 1993. Lateral stability of long prestressed concrete beams, Part 2. PCI Journal 38, 70–88.

Precast Concrete Association. Data Sheet for SY-beams.

Stratford, T.J., Burgoyne, C.J., 1999. The lateral stability of long precast concrete beams. Proc. Inst. Civil Engrs. 134, 169–180.

Stratford, T.J., Burgoyne, C.J., Taylor, H.P.J., 1999. The stability design of long precast concrete beams. Proc Inst Civil Engrs. 134, 159–168.

Swann, R.A., Godden, W.G., 1966. The lateral buckling of concrete beams lifted by cables. Struct. Engr 44, 21–33.